CrossMark

RESEARCH PAPER

Characterization of the PEGylated Functional Upstream Domain Peptide (PEG-FUD): a Potent Fibronectin Assembly Inhibitor with Potential as an Anti-Fibrotic Therapeutic

Pawel Zbyszynski[1] • Bianca R. Tomasini-Johansson[1] • Donna M. Peters[2] • Glen S. Kwon[1]

ABSTRACT

Purpose To develop PEGylated variants of pUR4/FUD (FUD), a fibronectin assembly inhibitor, using 10 kDa, 20 kDa, and 40 kDa PEGs to evaluate their binding affinity and inhibitory potency.

Methods The FUD peptide was recombinantly expressed, purified, and PEGylated at the N-terminus using 10 kDa, 20 kDa, and 40 kDa methoxy-PEG aldehyde. The PEGylates were purified and fractionated using ion-exchange chromatography. The molecular weight and degree of PEGylation of each conjugate was verified using MALDI-TOF. The binding affinity of each PEG-FUD conjugate was studied using isothermal titration colorimetry (ITC) and their inhibitory potency was characterized by a cell-based matrix assembly *in vitro* assay.

Results The 10 kDa, 20 kDa, and 40 kDa PEG-FUD conjugates were synthesized and isolated in good purity as determined by HPLC analysis. Their molecular weight was consistent with attachment of a single PEG molecule to one FUD peptide. The binding affinity (K_d) and the fibronectin fibrillogenesis inhibitory potency (IC50) of all PEG-FUD conjugates remained nanomolar and unaffected by the addition of PEG.

Conclusions Retention of FUD fibronectin binding activity following PEGylation with three different PEG sizes suggest that PEG-FUD holds promise as an effective anti-fibrotic with therapeutic potential and a candidate for further pharmacokinetic and biodistribution studies.

ABBREVIATIONS

70 K	70 kDa N-terminal region of fibronectin
ECM	Extracellular Matrix
FN	Fibronectin
FNI	Fibronectin type I domain
FUD	Functional Upstream Domain
ITC	Isothermal Titration Calorimetry
MAA	Matrix Assembly Assay
MALDI-	Matrix Assisted Laser Desorption/Ionization
TOF	Time of Flight
PEG	Polyethylene Glycol
TGF-β	Transforming Growth Factor β

INTRODUCTION

Fibrosis is a pathological condition characterized by excessive extracellular matrix (ECM) deposition by activated ECM-producing cells. Fibronectin (FN) is a prominent ECM component that is abundantly present in fibrotic tissue and represents a characteristic feature of this pathology. The deposition of FN precedes deposition of collagen and is important to the progression of fibrosis. The importance of FN is perhaps highlighted best by its involvement in processes that are instrumental to the development of fibrosis, like activation of Transforming Growth Factor β (TGF-β), deposition of collagens, and attachment of inflammatory lymphocytes (1–3). Because of these features, the deposition of FN is positioned

✉ Glen S. Kwon
gskwon@pharmacy.wisc.edu

[1] Division of Pharmaceutical Sciences, School of Pharmacy, University of Wisconsin-Madison, Madison, Wisconsin, USA

[2] Department of Pathology & Laboratory Medicine, School of Medicine and Public Health, University of Wisconsin-Madison, Madison, Wisconsin, USA

as a compelling therapeutic target for the treatment of the many forms of fibrosis.

FN is a 440–500 kDa dimeric vertebrate glycoprotein that is present in soluble form found circulating in blood and in fibrillar form found in interstitial tissues. There are two major FN isoforms: plasma FN synthesized by the liver and cellular FN that is synthesized locally by different cell types, including endothelial cells, myocytes, and fibroblasts [4]. In contrast to other ECM proteins, the assembly of FN structured fibrils (insoluble FN) is a cell mediated process which involves FN recognition by cell surface receptors such as integrins, elongation of its structure, and exposure of cryptic FN binding sites that are necessary for fibrillogenesis [5]. The N-terminal 70-kDa region (70 K) of FN is conserved between its isoforms and is critical to the assembly and ECM deposition of FN. Recombinant FN lacking some or all of [1-5]FNI 70 K domains is unable to form fibrils [6]. Pioneering research by *Mosher et al.* demonstrated that incubation of FN with the 70 K fragment can effectively block FN assembly through competitive inhibition of FN binding sites on the surfaces of fibroblasts [7]. Thus, because of the importance of FN assembly in progression of fibrosis, the N-terminal region of FN has become increasingly recognized as an attractive therapeutic target, leading to development of inhibitors exploiting blocking of FN fibrillogenesis.

Antibody and peptide inhibitors of FN fibrillogenesis targeting the N-terminal 30 K and 70 K regions of FN have been developed to successfully ameliorate the effects of fibrosis. In one study, Fn52RGDS, a 30 K targeting anti-FN antibody conjugated with an integrin binding FN sequence, RGDS, was found to be effective in causing a decline of fibrotic features in a fibrotic posterior capsular opacification model, a model used to study cataract formation [8]. This effect included a reduction in cell migration, fibronectin deposition, and collagen gel contraction. The decrease in fibrosis was most profound when the hybrid antibody was used in conjunction with the unmodified 30 K anti-FN antibody (Fn52), a synergism that achieved parity of effect while reducing required total drug quantity by an order of magnitude.

The Functional Upstream Domain (FUD) peptide, also referred to as pUR4, is another FN inhibitor shown to successfully relive the burden of fibrotic morphology. Part of the F1 adhesin protein of *Streptococcus pyogenes*, the Functional Upstream Domain (FUD) is a 6 kDa peptide that binds the [2-5]FNI and [8-9]FNI regions contained in the N-terminal 70 K of FN with nM affinity [9]. *In vitro* studies demonstrate that FUD is a potent inhibitor of exogenous FN fibril assembly and ECM deposition by various cell lines, such as hepatic stellate cells and dermal fibroblasts [10,11]. Application of the FUD peptide in a murine liver fibrosis model resulted in amelioration of deleterious effects of fibrosis, including reduction of tissue FN and collagen accumulation following injury without affecting their mRNA expression [11]. This difference resulted in a reduction of fibrotic tissue content as well as partial restoration of liver function. Together, the studies using Fn52RGDS and FUD act as proof of concept demonstrating FN inhibition as a successful therapeutic strategy for treating specific forms of fibrosis.

Because delivery of biologics is often challenged by elimination barriers like proteolysis and organ clearance that limit their systemic exposure [12–15], alternative delivery strategies for FUD were considered to maximize the peptide's therapeutic potential. This work explores PEGylation as a potential delivery strategy. PEGylation is a well-developed method known for improving delivery of biologics through enhancing their pharmacokinetic properties. To date, there exist at least ten PEGylated biologics that have been FDA approved and are currently on the US market [16]. PEGylation involves covalent attachment of a polyethylene glycol (PEG) moiety to a target molecule, thus increasing the drug's molecular weight and conferring PEG's characteristic large hydration sphere and hydrodynamic radius onto the drug. This enhancement can provide protection against enzymatic degradation, alter organ elimination by reducing renal filtration, and reduce generation of neutralizing antibodies [14]. The covalent attachment, however, can come at the cost of reducing affinity of the drug for its binding partner. Nevertheless, this cost is often therapeutically acceptable because of an overall increase in systemic exposure of the drug. In this work, FUD was conjugated with 10 kDa, 20 kDa, and 40 kDa PEG moieties, sizes that are expected to significantly diminish FUD affinity for FN. We intended to determine whether PEGylation would alter FUD binding affinity for FN and the inhibitory efficacy of fibronectin fibrillogenesis. Retaining strength of interaction would significantly increase the value of the therapeutic by improving FUD pharmacokinetics while avoiding the modification's undesirable effect.

Materials

Isopropyl β-D-1-thiogalactopyranoside, urea, imidazole, sodium chloride, calcium chloride, sodium phosphate, sodium acetate, tris(hydroxymethyl)aminomethane, sodium cyanoborohydride, fetal bovine serum, and Hank's Balanced Salt Solution with Ca^{2+} and Mg^{2+} were purchased from Sigma Aldrich (St Louis, USA). Tryptone, yeast extract, HPLC grade acetonitrile, and Alexa Fluor 488 were purchased from Thermo Fisher Scientific (Rockford, USA). Bovine alpha-Thrombin was purchased from Haematologic Technologies Incorporated (Essex Junction, USA). Human Plasma Fibronectin that has been purified by affinity chromatography on gelatin agarose and heparin agarose was purchased from EMD Millipore Corporation (Temecula, USA). Its concentration was determined from absorbance measurements at 280 nm and $\varepsilon = 1.3$ as described by the manufacturer's specifications. CellTiter-Glo was purchased from

Promega (Madison, USA). The methoxy-PEG10K-aldehyde, methoxy-PEG20K-aldehyde, and methoxy-PEG40K-aldehyde were purchased from NOF Corporation (Kawasaki, Japan). All solvents and chemicals used in this study were of analytical grade.

AH1F cells are human foreskin fibroblasts characterized as previously described (17).

PROCEDURE

FUD and mFUD Synthesis

The FUD peptide and its mFUD control peptide variant (18) were recombinantly expressed in BL21 (DE3) *E. coli* as a His-tagged pET-ELMER construct using previously described protocol (9) with modifications recently reported by *Filla et al.* pertaining to His-tag removal (18). Briefly, expression of FUD or mFUD was induced by 1 mM isopropyl β-D-1thiogalactopyranoside and cell lysis was facilitated by a lysis buffer (100 mM Sodium Phosphate, 10 mM Tris, 8 M Urea, 5 mM imidazole, pH 8.0). The lysate was cleared of particulates via centrifugation and incubated overnight with Ni-NTA agarose (Qiagen). The Ni-NTA agarose was washed three times with a washing buffer (100 mM Sodium Phosphate, 10 mM Tris, 8 M Urea, 5 mM imidazole, pH 8.0) and three more times with an elution buffer (20 mM Tris, 150 mM NaCl, 2.5 mM $CaCl_2$, pH 8.4). Elution of FUD and removal of the His tag was achieved by using a thrombin cleavage site between the His-tag and FUD. For this, FUD bound to the Ni-NTA agarose was incubated with 1 unit of Bovine α-Thrombin per 1 mg of expressed peptide. The peptide was further purified via fast protein liquid chromatography (FPLC) using HiTrap Q HP column as described in the PEG-FUD Purification section. Peptide identity was verified via UPLC-ESI ultra high resolution QTOF MS. The concentration of FUD and PEG-FUD conjugates were obtained with absorbance measurements at 280 nm using ε = 0.496 as described previously (9). The concentration of mFUD was determined similarly using ε = 0.744.

Preparation of PEGylated FUD and mFUD

PEGylation and subsequent FPLC purification were carried out using the same procedure for all constructs. The FUD or mFUD peptide was incubated with 10 kDa and 20 kDa linear or 40 kDa branched methoxy-PEG propionaldehyde (NOF, Japan) in 50 mM Sodium Acetate buffer (pH 5.5). All materials were dissolved in or exchanged via dialysis into the appropriate buffer prior to mixing. The reaction was carried out in the presence of 26.7 mM $NaCNBH_3$ for 16 h at 4°C. Final FUD peptide concentration of 0.63 mg/mL was used with a FUD:PEG molar ratio of 1:10. The

polydispersity of the PEG reagent was 1.04, 1.02, and 1.06 for 10 kDa, 20 kDa, and 40 kDa PEG, respectively. After 16 h reaction time, the reducing agent was removed via dialysis in 50 mM Sodium Acetate buffer (pH 5.5). The buffer was switched after 1 and 4 h, and then exchanged for 20 mM Tris (pH 8.0) for 3 more hrs.

FPLC Separation and Purification of PEGylated FUD and mFUD

The PEG-FUD or PEG-mFUD reaction mixture was loaded onto a HiTrap Q HP anion exchange column (GE Healthcare Life Sciences, USA) initially equilibrated with Buffer A (20 mM Tris, pH 8.0). Upon sample injection, the column was washed with 2 CVs of Buffer A and the sample was eluted with a 10 CV gradient of Buffer B (1 M NaCl in 20 mM Tris, pH 8.0) at a flow rate of 3.5 mL/min. The fraction containing PEG-FUD was collected, concentrated using Amicon Ultra-15 3000 MWCO Centrifugal Filter Units (MilliporeSigma), and snap frozen. Routine purity assessment was carried out using RP-HPLC.

GPC Characterization

FUD and 10 kDa, 20 kDa, and 40 kDa PEG-FUD were loaded onto a TSKgel G4000PW$_{XL}$ Column (TOSOH Bioscience) connected to a 1100 Series (Agilent) system and equilibrated and eluted with 10 mM Phosphate Buffer (pH 7.4) at a flow rate of 1 mL/min. A typical run was allowed to proceed for 30 min. A DAD detector set to 280 nm was used to detect the peptides.

HPLC Characterization

Purified FUD and 10 kDa, 20 kDa, and 40 kDa PEG-FUD peptides were loaded onto a Zorbax SB-C8 4.6 × 75 mm column with a 3.5 µm pore size (Agilent) connected to a Prominence UFLC system (Shimadzu). A water/acetonitrile elution gradient with a flow rate of 1 mL/min was used to separate the sample. A typical run was allowed to proceed for 46 min. Absorbance at 280 nm was used to detect the peptides.

MALDI-TOF MS Characterization of PEG-FUD

Prior to analysis, the peptide complexes were dialyzed overnight into deionized H_2O using a 3000 MWCO dialysis membrane. The samples were then purified on Omix C18 Tips according to the manufacturer's protocol (Agilent). Purified PEGylated peptides were then mixed 1:1 with 10 mg/mL α-cyano-4-hydroxycinnamic acid (1 µL analyte and matrix) and analyzed on UltraFleXtreme MALDI-TOF (Bruker) mass spectrometer in positive ion, linear mode.

ITC Characterization

ITC experiments were performed using a VP-ITC microcalorimeter (MicroCal, LLC) with a cell volume of 2.2 mL. In a typical experiment, the cell was filled with 1.4 mL of 2 μM human plasma FN and the syringe was filled with 1 mL of 28 μM FUD or PEG-FUD peptides. The temperature was set to 25°C. The titration experiment was performed in 39 injections (1×1, 4×4, and 34×8 μL) delivered in 120 s intervals. Prior to injection, both FN and the peptides were dialyzed in separate dialysis bags overnight into the same PBS buffer (pH 7.4) solution. Routine analysis involved discarding of the first data point and subtraction of peptide into PBS buffer control run. Data were fit using one set of sites model Lavenberg-Marquardt nonlinear regression in Origin 7.0.

Matrix Assembly Assay

The matrix assembly assay was conducted in the 96-well plate format as described previously [17]. AH1F human skin fibroblast cells resuspended in 2% fetal bovine serum were added to each well for a density of 60,000 cells per well. A 1 h incubation period at 37°C followed to allow cell adhesion and spreading. FUD, PEG-FUD, or PEG-mFUD were added to each well following incubation. Immediately, Alexa Fluor 488 fluorescence labeled human plasma fibronectin (A488-FN) was then added to each well for a final FN concentration of 11 μg/mL. The cells were then incubated for 24 h at 37°C. Nonassembled FN was removed from each well by washing with Hank's Balanced Salt Solution (HBSS) containing Ca^{2+} and Mg^{2+}. The well volume was restored to 60 μL with HBSS and a fluorescence reading from the bottom of each well was taken using a Synergy H1 (Biotek) plate reader (excitation: 485 nm, Emission: 538 nm). Cell viability was quantified using CellTiter-Glo cell viability assay using the manufacturer's protocol. A 30 μL aliquot of HBSS was removed from each well and was replaced with 30 μL of the luminescence reagent prepared shortly beforehand. Luminescence was quantified using the same plate reader. The average of fluorescence values of a no A488FN or inhibitor control group were routinely subtracted from the readings of each well and were normalized using each well's corresponding luminescence value. Lastly, the cell viability normalized fluorescence values were expressed as a percentage of the 0 nM drug control group. The final results were processed using Graphpad Prism 7.0 software. IC50 values were extracted using a four-parameter dose-response curve function. Student's t test was used to determine significance of differences among peptides at a given drug concentration.

RESULTS

PEG-FUD Synthesis

The FUD peptide and a mutated FUD control peptide, termed mFUD, were successfully expressed using recombinant technology as described previously [9,18]. Peptide expression was induced using IPTG at a colony optical density of 0.6, approximately 4 h following colony seeding. In a typical experiment, a 6 L batch was created to recover 8 mg of FUD or 3 mg of mFUD per liter of cell culture medium. Ion exchange chromatography was used as the final purification step following Ni-NTA agarose His-tag purification. A singular peak corresponding to the FUD or mFUD peptide eluted at 33.0 %B and 33.3 %B, respectively, when an anionic exchanger was used (SM 1). The isolate identity was verified using LC-MS, agreeing with the theoretical mass of the FUD peptide (6003.820025 Da) within 1.4 ppm mass accuracy and within 0.15 ppm mass accuracy for the mFUD peptide (6024.78754 Da).

The 10 kDa, 20 kDa, and 40 kDa PEGylated FUD constructs were synthesized using reductive addition chemistry (Fig. 1) shown previously to be N-terminus specific using proteolytic digests in tandem with HPLC and/or MALDI-TOF analysis [19–21]. This reaction chemistry targets primary amines present in the peptide to covalently attach a PEG moiety via its aldehyde functionality. The more reactive α-amino group of the N-terminal residue of the peptide is preferentially targeted at low pH in this reaction strategy because of its lower pK_a (7.6–8.0) compared to other amines present in the peptides, including ϵ-amino groups of Lys residues (10.0–10.2) [22]. After reaction time optimization, a 16 h method was chosen for most efficient production of PEG-FUD constructs, selecting for a maximal FPLC PEG-FUD peak height. As shown in Fig. 2, the generated 10 kDa, 20 kDa, and 40 kDa PEG-FUD final conjugates eluted at 25.8 %B, 23.8 %B and 19.6 %B, respectively, upon ion exchange chromatography purification and were separated from unreacted FUD, PEG, and other species by fractionation.

In addition to synthesizing a set of PEG-FUD peptide variants, the mFUD control peptide was also PEGylated using 20 kDa methoxy-PEG propionaldehyde to function as a control peptide for *in vitro* efficacy experiments. The same procedure was used to create this construct as with all PEG-FUD variants. A similar reaction species distribution and anion exchange elution profile was observed between 20 kDa PEG-mFUD and 20 kDa PEG-FUD. An ion-exchange elution chromatogram is presented in SM 2. Analysis via RP-HPLC revealed the retention time of mFUD increasing from 13.259 min to 21.988 min upon PEGylation with 20 kDa PEG (SM 3). This retention time compares to 21.984 min of the 20 kDa PEG-FUD conjugate.
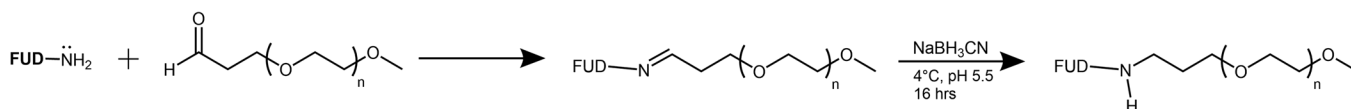
Fig. 1 N-terminus specific chemistry was used to synthesize 10 kDa, 20 kDa, and 40 kDa PEG-FUD conjugates.

PEG-FUD Characterization

Gel Permeation Chromatography (GPC) and Reversed Phase High Performance Liquid Chromatography (RP-HPLC) analysis yielded singular peaks for each PEG-FUD construct, confirming sample purity, with shifted retention times and peak broadening characteristic of conjugation with a polydisperse PEG polymer. Upon attachment of a PEG moiety, the GPC analysis retention time of FUD decreased from 11.516 min to 10.893 min, 10.583 min, and 10.160 min for 10 kDa, 20 kDa, and 40 kDa PEG-FUD, respectively (Fig. 3). RP-HPLC analysis yielded a FUD retention time increase from 12.800 min to 20.602 min, 21.984 min, and 23.461 min for 10 kDa, 20 kDa, and 40 kDa PEGylated conjugates, respectively (Fig. 4). Together, the two analytical techniques suggest covalent modification of FUD with a PEG moiety. The degree of PEGylation of the three PEG-FUD conjugates was verified using Matrix-Assisted Laser Desorption/Ionization Mass Spectrometry (MALDI-MS).

The nominal molecular weight of the 20 kDa PEG-FUD conjugate was determined to be 27,390 Da using this technique (Fig. 5). This weight corresponds to attachment of one PEG unit (21,304 Da) to the FUD peptide (6004 Da). The nominal molecular weights of the PEG-FUD conjugates generated with 10 kDa and 40 kDa PEGs were similarly characterized and determined to be 16,946 Da and 49,582 Da, respectively, corresponding to attachment of one PEG unit (11,096 Da and 43,667 Da) to the FUD peptide (SM 4 and 5). This technique was also used to ascertain the mass of the PEG-mFUD conjugate (SM 6). As expected, a nominal mass of 27,400 Da was observed. Together, the GPC, RP-HPLC, and MALDI-TOF MS data demonstrate successful synthesis and isolation of the PEG-FUD and PEG-mFUD peptides.

PEG-FUD Binding Studies

The binding of 10 kDa, 20 kDa, and 40 kDa PEG-FUD to FN was studied using Isothermal Titration Calorimetry (ITC). This technique was used to determine the thermodynamic parameters as well as the binding constant (K_d) of the interaction. The peptide was injected into a human plasma FN solution in PBS at pH 7.4 and 25°C in triplicate runs. Sample FUD and 20 kDa PEG-FUD into fibronectin ITC isotherms and thermographs are presented in Fig. 6. ITC results of additional conjugates are available in SM 7. The overall thermodynamic binding parameters are summarized and presented in Table I. Similar binding affinity and binding parameters were observed for both the peptide and its PEGylated constructs. A K_d of 6 (± 3) nM was detected for FUD:FN. Similarly, a K_d of 4.6 (± 0.5) nM was detected for 10 kDa PEG-FUD:FN, 10 (± 2) nM for 20 kDa PEG-FUD:FN, and 14.7 (± 0.9) nM for 40 kDa PEG-FUD:FN interactions. Similar entropy change of -65 (± 3) cal/mol, -74 (± 7) cal/mol, -66 (± 7) cal/mol, and -73 (± 2) and enthalpy change of -31 (± 1) kcal/mol, -34 (± 2) kcal/mol, -30 (± 1) kcal/mol, and -32.5 (± 0.5) kcal/mol were detected for the interaction of FUD and 10 kDa, 20 kDa, and 40 kDa PEG-FUD with FN, respectively. Together, these findings indicate that the tight nanomolar binding affinity as well as the overall interaction of FUD for FN is not significantly affected by N-terminal

Fig. 2 FPLC ion exchange chromatogram showing isolation by fractionation of the 10 kDa, 20 kDa, and 40 kDa PEG-FUD constructs. An anionic exchanger combined with a mobile phase gradient of 20 mM Tris A side and 1 M NaCl B side were used to elute the peptide and separate it from unreacted FUD, PEG, and diPEGylated species.
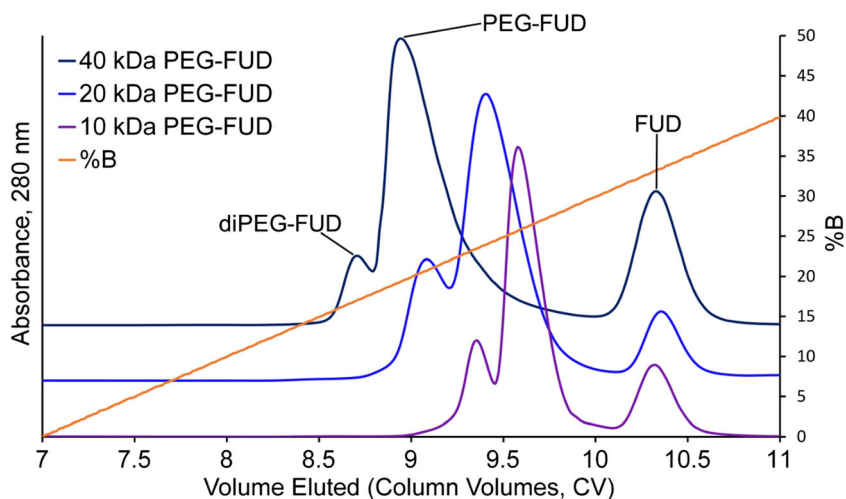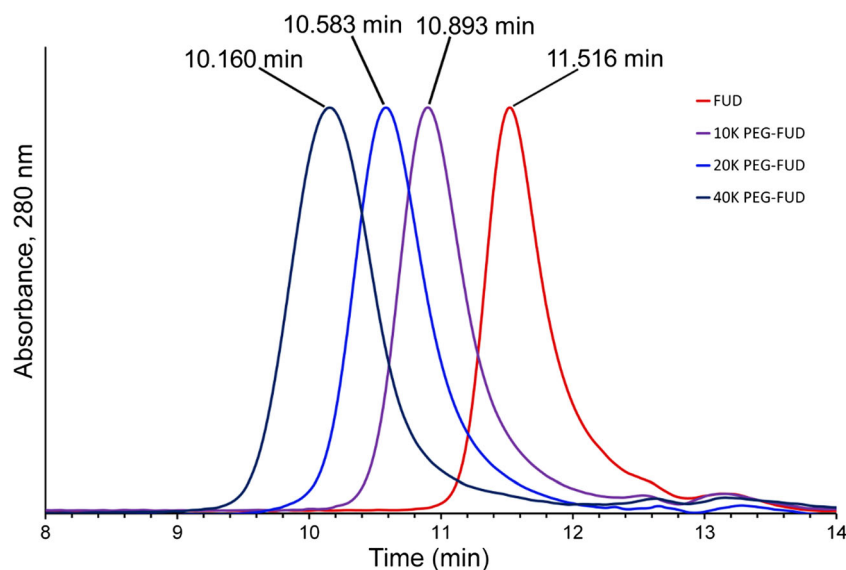
Fig. 3 Gel Permeation Chromatography (GPC) experiments reveal reduced 10 kDa, 20 kDa, and 40 kDa PEG-FUD retention times and suggest increase in molecular weight of FUD upon PEGylation. Experiments were done using 10 mM pH 7.4 Phosphate Buffer mobile phase.

covalent attachment with a PEG moiety. This observation is contrary to the expectation of PEG attachment diminishing a drug's affinity for its binding partner (14) and presents an unexpected but desired feature of the PEG-FUD peptide.

The PEG-FUD FN fibrillogenesis inhibitory performance was evaluated *in vitro* using the matrix assembly assay (MAA) (17). The methodology of this assay is depicted in Fig. 7a. The MAA quantifies ECM deposition of exogenous Alexa 488-labeled FN (A488FN) by a confluent monolayer of fibroblasts after an incubation period by measuring fluorescence of deposited FN. In this study, the performance of PEG-FUD peptides was compared to that of FUD and the PEG-mFUD control peptide using the AH1F human foreskin fibroblast cell line. As shown in Fig. 7b, the normalized fluorescence intensity of the PEG-mFUD control peptide group was found to be maximal and with no statistically significant differences from the 0 nM control group. This concentration independence

indicates that the PEG-mFUD peptide demonstrates no FN fibrillogenesis inhibition over the concentration range studied (0–250 nM). The cell viability normalized fluorescence intensity of FUD, 10 kDa PEG-FUD, 20 kDa PEG-FUD, and 40 kDa PEG-FUD experimental groups rapidly declined with increasing peptide concentration. The calculation of IC50 values produced an IC50 of 17 nM for 10 kDa PEG-FUD *vs* 13 nM of FUD, 23 nM for 20 kDa PEG-FUD *vs* 26 nM of FUD (Fig. 7b), and 20 nM for 40 kDa PEG-FUD *vs* 19 nM of FUD. Results of 10 kDa and 40 kDa MAA experiments are available in SM 8a and 8b. As ascertained by student's t-test, the means of cell viability normalized fluorescence intensity values at each drug concentration for the three PEGylated peptides were not significantly different from those of FUD. The PEGylated FUD conjugates thus showed a parity of inhibitory performance compared to FUD. This experiment demonstrates that despite PEGylation, the 10 kDa, 20 kDa

Fig. 4 Reversed Phase High Performance Liquid Chromatography (RP-HPLC) chromatograph showing an increase of FUD retention time after PEGylation. The analysis was made using a C8 column combined with an A side H_2O and B side acetonitrile mobile phase elution gradient.
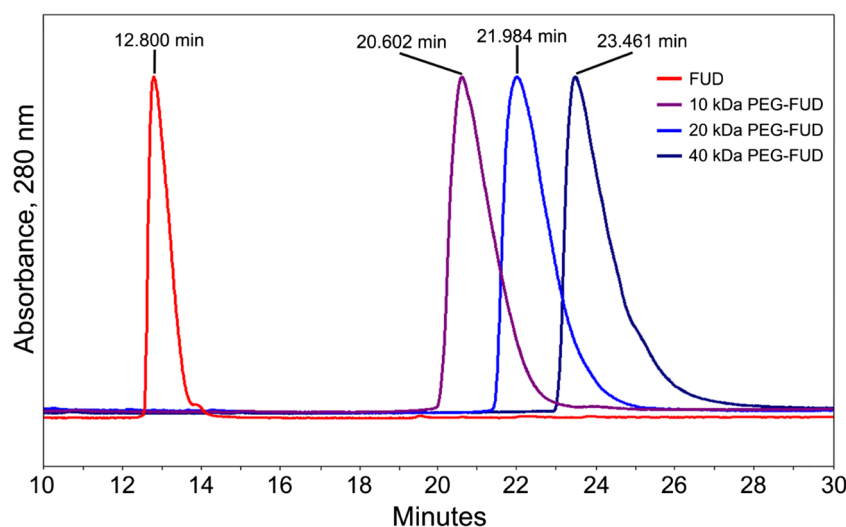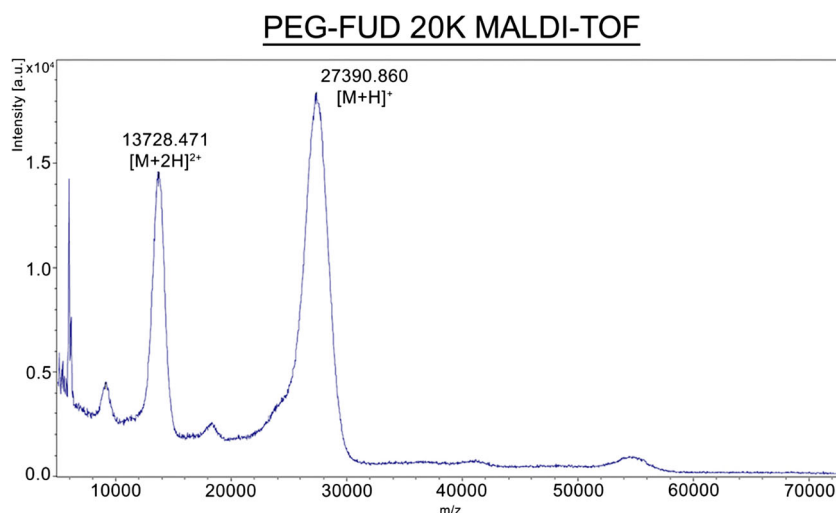
Fig. 5 MALDI-TOF MS spectrum verifying the molecular weight of the 20 kDa PEG-FUD construct. A 6 kDa FUD reacted with a single 21.3 kDa nominal MW PEG to yield a 27.3 kDa PEG-FUD. The analysis was made using α-cyano-4-hydroxycinnamic acid matrix.

and 40 kDa PEG-FUD constructs retain FUD's strong ability to inhibit FN fibril assembly. These MAA findings complement ITC experiments verifying a parity of binding affinity. Together, the ITC and MAA data both demonstrate that the PEGylated FUD constructs are equally potent FN fibrillogenesis inhibitors and that PEGylated mFUD is a valid control peptide.

DISCUSSION

Size-dependent reduction in renal clearance following PEGylation is one of the primary drivers of pharmacokinetic improvement that was leveraged in designing an enhanced FUD peptide. In order for this approach to be effective, however, an optimally sized PEG had to be selected for the reduction in filtration of the glomerulus of the kidney to be sufficiently significant (14,23,24). Studies tracking ^{125}I-labeled PEG of different sizes after i.v. infusion point to urinary clearance of PEG abruptly decreasing around the molecular weight of 30 kDa (25). Another study reinforces these findings with an immunohistochemical approach. Upon i.v. infusion, PEG immunoreactivity in the proximal renal tubules was found to diminish accordingly with PEG sizes of 10 kDa, 20 kDa, and 40 kDa, reiterating the size dependence of glomerular penetration (26). These observations were used to select PEG sizes of 10 kDa, 20 kDa, and 40 kDa for PEGylation of the FUD peptide. The design intended for

Fig. 6 Determination of binding affinity (K_d) and other thermodynamic parameters using Isothermal Titration Calorimetry (ITC). All experiments were performed using pH 7.4 PBS, 25°C chamber conditions, and human plasma FN. A) FUD into FN and B) 20 kDa PEG-FUD into FN experiment sample isotherm and thermograph. Each experiment was repeated in triplicates.
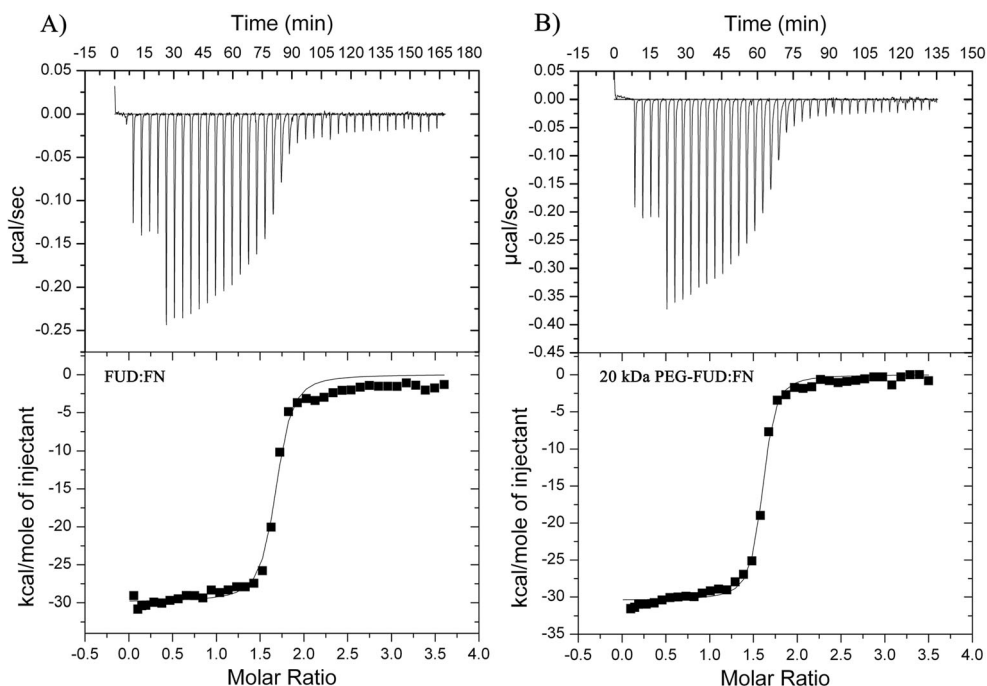
Table I ITC Binding Parameters

Interaction	[FN] μM	[Peptide] μM	T °C	n	Kd nM	ΔG kcal mol^{-1}	ΔH kcal mol^{-1}	ΔS cal mol^{-1}
FUD:FN	1.7–1.8	23–29	25	1.59	6	−11.4	−31	−65
stdev				0.06	3	0.3	1	3
10 K PEG-FUD:FN	2.0–2.4	37–38	25	1.55	4.6	−11.39	−34	−74
stdev				0.06	0.5	0.09	2	7
20 K PEG-FUD:FN	1.0–2.7	25–42	25	1.63	10	−10	−30	−66
stdev				0.07	2	1	1	7
40K PEG-FUD-FN	1.8–2.0	28.8	25	1.43	14.7	−10.91	−32.5	−73
stdev				0.05	0.9	0.02	0.5	2

the individual constructs to have a nominal molecular weight that is smaller (~16.9 kDa), intermediately sized (~27.4 kDa), and large (~49.6 kDa). This diversity of molecular weights provides therapeutic candidates with increasingly reduced renal filtration behavior, expecting for the larger 40 kDa PEG-FUD to gain greatest plasma residence time improvements. The size of the PEG-FUD constructs was thus chosen strategically. The retention of low nanomolar binding affinity and parity of inhibitory potency reported in this work combined with FUD anti-fibrotic success reported previously (11) stress

the importance of evaluating this PEG-FUD library in an animal model of fibrosis for efficacy and pharmacokinetic performance to correlate PEG-FUD size with desired performance.

While the method of PEG conjugation was chosen with intent of minimizing PEGylation related binding affinity reduction, it was unexpected for a parity of inhibitory potency to be observed between FUD and PEG-FUD peptides. There exist numerous examples of PEGylation diminishing its target's activity. This reduction can vary from notable (PEG-

Fig. 7 Matrix Assembly *in vitro* Assay (MAA) demonstrating inhibitory potency of FUD and 20 kDa PEG-FUD conjugates, and the 20 kDa PEG-mFUD control peptide. (**a**) Schematic representation of assay methodology. Human foreskin fibroblasts (AH1F) are grown in the presence of exogenous Alexa 488-labeled human plasma FN and in the presence or absence of an inhibitor. (**b**) Results of a MAA experiment comparing 20 kDa PEG-FUD to FUD and showing parity of inhibitory potency. Extraction of IC50 values yielded 26 nM and 23 nM for FUD and 20 kDa PEG-FUD, respectively. For each data point, $n = 4$.
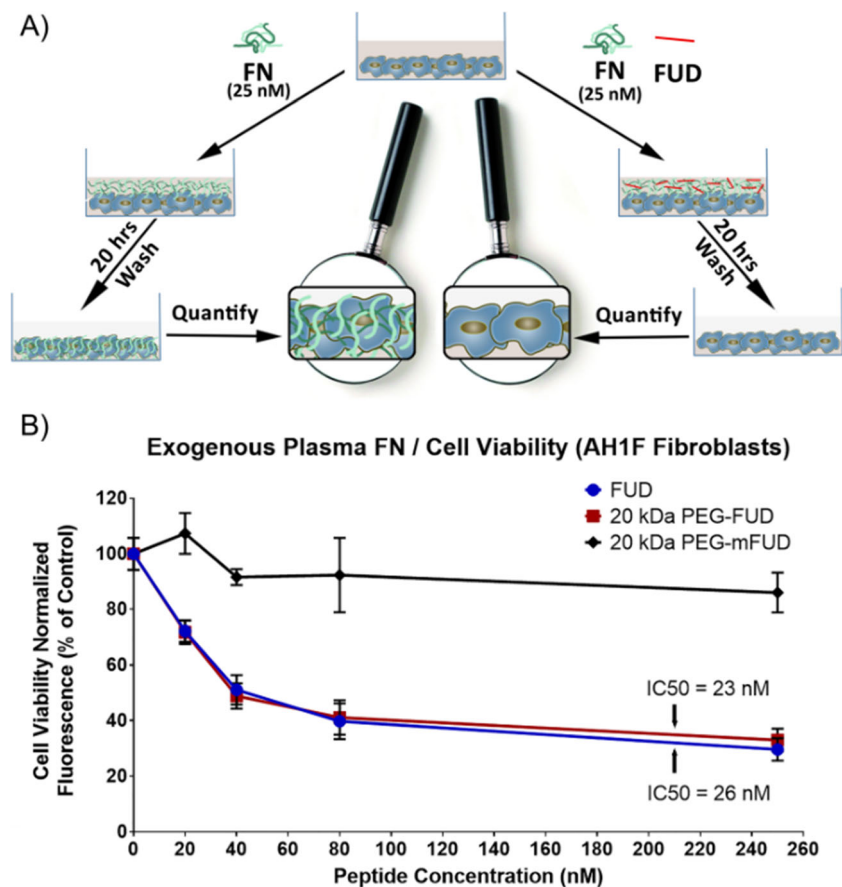
IFN-α2b: 3.6 fold (27), PEG$_2$-IFN: 14 fold (28), PEG-B2036: 28 fold (29)), to reducing activity by several orders of magnitude (PEG-G120 K-GH: 186 fold (29)). Some causes of this effect include disruption of the target's secondary structure and thus its binding motif, and steric interference of the binding site via proximal conjugation. First, the case of secondary structure modification of the peptide did not require mitigation because FUD is an unstructured peptide that assumes a random coil conformation when in solution (9). However, because FUD assumes beta strand conformation upon binding with FN, the nature of the ligand/target interaction opens the possibility of secondary structure interference by a PEG spectator. This possibility contributed to uncertainty in predicting the binding affinity of PEG-FUD. Secondly, the site of PEGylation (i.e. N-terminus) was chosen specifically to minimize the risk of a PEG conjugation that is proximal to FUD's binding site for FN. Research suggests that FUD binding to FN involves many residues that are located along an extensive part of the peptide that together contribute to the peptide's tight nanomolar avidity for the 70 K region of FN (9). It was intended for N-terminal PEGylation to be far removed from the core of this interaction, thus reducing the possibility of steric interference and leaving more C-terminal residues unrestricted to bind FN. It was suspected, however, that some binding affinity reduction was unavoidable because previous research suggested that the N-terminus of FUD may be involved in the peptide's interaction with FN (9). Furthermore, when bound to FN, the N-terminus tail of FUD is positioned facing the central portion of FN. Thus, a large PEG moiety conjugated at the N-terminus of FUD is liable to interfere with the dynamic folding and interactions of FN domains, potentially disturbing the binding of FUD to FN. These two concerns thus illustrate why this work's findings are surprising. The retained low nanomolar binding affinity and unaffected FN fibrillogenesis inhibitory potency of PEG-FUD is unexpected and presents a unique property of the FUD peptide that can be exploited in applications using FN as a therapeutic target but for which the nature of peptide pharmacokinetics reduces FUD usefulness as a therapeutic candidate.

Organ fibrosis and fibrosis-associated progression of cancer are two application spaces in which a PEGylated fibronectin inhibitor may hold added therapeutic potential. The success of FUD fibronectin inhibition therapy in a mouse model of liver fibrosis (11) suggests that this approach may be applied to other models of fibrosis that involve less accessible organs than the liver if the drug's pharmacokinetic properties are appropriately adjusted. Administration of a PEGylated FUD variant has the potential of improving FUD penetration into the kidneys by increasing the drug's circulation time, thus pointing to PEG-FUD as a potential therapeutic for the treatment of renal fibrosis. Recently published work suggesting that structural alterations of peritubular capillaries associated with renal fibrosis allow increased extravasation of solutes as large as albumin

(65–70 kDa) and fibrinogen (340 kDa) into the peritubular interstitum (30,31) also present a tantalizing possibility for improved delivery of a long circulating therapeutic with an enhanced molecular weight. Previous successes, combined with this observation, stress the importance of PEG-FUD therapeutic efficacy evaluation in the renal fibrosis context.

Fibrosis-associated progression of cancer also presents an area of research for which PEG-FUD could be a strong therapeutic candidate. Fibronectin and collagens have been implicated in the growth, migration, and invasion ability of a variety of tumors. Research has shown that fibrotic tissue is associated with a predisposition for development of both lung cancer (32) and breast cancer (33). This concept is especially relevant to cancer cell shedding and development of metastasis in fibronectin-rich tissue. For example, this "priming the soil" effect has been observed with ovarian cancer cells secreting TGFβ, thereby inducing secretion of fibronectin by mesothelial cells which in turn facilitate adhesion, proliferation, and metastasis of ovarian cancer (34). Other research has shown that colonization of circulating breast cancer 4 T1 tumor cells is doubled in two models of lung fibrosis and increased by 50% in one model of liver fibrosis (35). These findings suggest value in evaluation of fibronectin inhibition as a strategy for metastasis mitigation. A PEGylated FUD peptide with equal potency but tailored pharmacokinetic profile may be a very useful tool in studying this therapeutic strategy against fibrotic cancers.

CONCLUSION

The FUD peptide was successfully conjugated with 10 kDa, 20 kDa, or 40 kDa PEG moieties and isolated in good purity. The mass of the PEG-FUD constructs agreed with attachment of a single PEG molecule. Unexpectedly, retention of low nanomolar binding affinity was found following PEGylation with all three constructs. Furthermore, all three PEG-FUD peptides were found to be equally effective at inhibiting FN fibrillogenesis *in vitro* compared to unmodified FUD. These results suggest anti-fibrotic value of this peptide and stress the importance of evaluation of these PEG-FUD constructs in the context of therapeutic efficacy and pharmacokinetic performance in an animal model of fibrosis.

ACKNOWLEDGMENTS AND DISCLOSURES

REFERENCES

1. Sottile J, Hocking DC. Fibronectin polymerization regulates the composition and stability of extracellular matrix fibrils and cell-matrix adhesions. Mol Biol Cell. 2002;13(10):3546–59.

2. Dallas SL, Sivakumar P, Jones CJP, Chen Q, Peters DM, Mosher DF, et al. Fibronectin regulates latent transforming growth factor-β (TGFβ) by controlling matrix assembly of latent TGFβ-binding Protein-1. J Biol Chem. 2005;280(19):18871–80.

3. Moore C, Shen X-D, Gao F, Busuttil RW, Coito AJ. Fibronectin-α4β1 integrin interactions regulate Metalloproteinase-9 expression in Steatotic liver ischemia and reperfusion injury. Am J Pathol. 2007;170(2):567–77.

4. Maurer LM, Ma W, Mosher DF. Dynamic structure of plasma fibronectin. Crit Rev Biochem Mol Biol. 2016;51(4):213–27.

5. Singh P, Carraher C, Schwarzbauer JE. Assembly of fibronectin extracellular matrix. Annu Rev Cell Dev Biol. 2010;26:397–419.

6. Schwarzbauer JE. Identification of the fibronectin sequences required for assembly of a fibrillar matrix. J Cell Biol. 1991;113(6):1463–73.

7. McKeown-Longo PJ, Mosher DF. Interaction of the 70,000-Mol-wt amino-terminal fragment of fibronectin with the matrix-assembly receptor of fibroblasts. J Cell Biol. 1985;100(2):364–74.

8. Tiwari A, Kumar R, Ram J, Sharma M, Luthra-Guptasarma M. Control of fibrotic changes through the synergistic effects of anti-fibronectin antibody and an RGDS-tagged form of the same antibody. Sci Rep. 2016;6:30872.

9. Maurer LM, Tomasini-Johansson BR, Ma W, Annis DS, Eickstaedt NL, Ensenberger MG, et al. Extended binding site on fibronectin for the functional upstream domain of protein F1 of Streptococcus pyogenes. J Biol Chem. 2010;285(52):41087–99.

10. Tomasini-Johansson BR, Kaufman NR, Ensenberger MG, Ozeri V, Hanski E, Mosher DF. A 49-residue peptide from Adhesin F1 of Streptococcus pyogenes inhibits fibronectin matrix assembly. J Biol Chem. 2001;276(26):23430–9.

11. Altrock E, Sens C, Wuerfel C, Vasel M, Kawelke N, Dooley S, et al. Inhibition of fibronectin deposition improves experimental liver fibrosis. J Hepatol. 2015;62(3):625–33.

12. Weinstock MT, Francis JN, Redman JS, Kay MS. Protease-resistant peptide design—empowering nature's fragile warriors against HIV. Pept Sci. 2012;98(5):431–42.

13. McGregor DP. Discovering and improving novel peptide therapeutics. Curr Opin Pharmacol. 2008;8(5):616–9.

14. Fishburn CS. The pharmacology of PEGylation: balancing PD with PK to generate novel therapeutics. J Pharm Sci. 2008;97(10):4167–83.

15. Tang L, Persky AM, Hochhaus G, Meibohm B. Pharmacokinetic aspects of biotechnology products. J Pharm Sci. 2004;93(9):2184–204.

16. Li W, Zhan P, De Clercq E, Lou H, Liu X. Current drug research on PEGylation with small molecular agents. Prog Polym Sci. 2013;38(3):421–44.

17. Tomasini-Johansson BR, Johnson IA, Hoffmann FM, Mosher DF. Quantitative microtiter fibronectin fibrillogenesis assay: use in high throughput screening for identification of inhibitor compounds. Matrix Biol. 2012;31(6):360–7.

18. Filla MS, Dimeo KD, Tong T, Peters DM. Disruption of fibronectin matrix affects type IV collagen, fibrillin and laminin deposition into extracellular matrix of human trabecular meshwork (HTM) cells. Exp Eye Res. 2017;165:7–19.

19. Lee S-H, Lee S, Youn YS, Na DH, Chae SY, Byun Y, et al. Synthesis, characterization, and pharmacokinetic studies of PEGylated glucagon-like Peptide-1. Bioconjug Chem. 2005;16(2):377–82.

20. Kinstler OB, Brems DN, Lauren SL, Paige AG, Hamburger JB, Characterization TMJ. Stability of N-terminally PEGylated rhG-CSF. Pharm Res. 1996;13(7):996–1002.

21. Guerra PI, Acklin C, Kosky AA, Davis JM, Treuheit MJ, Brems DN. PEGylation prevents the N-terminal degradation of megakaryocyte growth and development factor. Pharm Res. 1998;15(12):1822–7.

22. Kinstler O, Molineux G, Treuheit M, Ladd D, Gegg C. Mono-N-terminal poly(ethylene glycol)–protein conjugates. Adv Drug Deliv Rev. 2002;54(4):477–85.

23. Pasut G, Veronese FM. State of the art in PEGylation: the great versatility achieved after forty years of research. J Control Release. 2012;161(2):461–72.

24. Harris JM, Chess RB. Effect of pegylation on pharmaceuticals. Nat Rev Drug Discov. 2003;2(3):214–21.

25. Yamaoka T, Tabata Y, Ikada Y. Distribution and tissue uptake of poly(ethylene glycol) with different molecular weights after intravenous administration to mice. J Pharm Sci. 1994;83(4):601–6.

26. Rudmann DG, Alston JT, Hanson JC, Heidel S. High molecular weight polyethylene glycol cellular distribution and PEG-associated cytoplasmic Vacuolation is molecular weight dependent and does not require conjugation to proteins. Toxicol Pathol. 2013;41(7):970–83.

27. Wang Y-S, Youngster S, Grace M, Bausch J, Bordens R, Wyss DF. Structural and biological characterization of pegylated recombinant interferon alpha-2b and its therapeutic implications. Adv Drug Deliv Rev. 2002;54(4):547–70.

28. Bailon P, Palleroni A, Schaffer CA, Spence CL, Fung W-J, Porter JE, et al. Rational Design of a Potent, long-lasting form of interferon: a 40 kDa branched polyethylene glycol-conjugated interferon α-2a for the treatment of hepatitis C. Bioconjug Chem. 2001;12(2):195–202.

29. Ross RJM, Leung KC, Maamra M, Bennett W, Doyle N, Waters MJ, et al. Binding and functional studies with the growth hormone receptor antagonist, B2036-PEG (Pegvisomant), reveal effects of Pegylation and evidence that it binds to a receptor Dimer1. J Clin Endocrinol Metab. 2001;86(4):1716–23.

30. Bábíčková J, Klinkhammer BM, Buhl EM, Djudjaj S, Hoss M, Heymann F, et al. Regardless of etiology, progressive renal disease causes ultrastructural and functional alterations of peritubular capillaries. Kidney Int. 2017;91(1):70–85.

31. Ehling J, Bábíčková J, Gremse F, Klinkhammer BM, Baetke S, Knuechel R, et al. Quantitative micro-computed tomography imaging of vascular dysfunction in progressive kidney diseases. J Am Soc Nephrol. 2016;27(2):520–32.

32. MOSSMAN BT, CHURG A. Mechanisms in the pathogenesis of asbestosis and silicosis. Am J Respir Crit Care Med. 1998;157(5):1666–80.

33. Coughlin MK. Radial scars in benign breast-biopsy specimens and the risk of breast Cancer. AORN J. 2000;71(1):240–2.

34. Kenny HA, Chiang C-Y, White EA, Schryver EM, Habis M, Romero IL, et al. Mesothelial cells promote early ovarian cancer metastasis through fibronectin secretion. J Clin Invest. 2014;124(10):4614–28.

35. Cox TR, Bird D, Baker A-M, Barker HE, Ho MWY, Lang G, et al. LOX-mediated collagen crosslinking is responsible for fibrosis-enhanced metastasis. Cancer Res. 2013;73(6):1721–32.